

## The effects of central metals on ammonia sensing of

### metallophthalocyanines covalently bonded to graphene Oxide hybrids†

Yong Li<sup>a</sup>, Bin Wang<sup>\*a</sup>, Zheying Yu<sup>a</sup>, Xiaoqing Zhou<sup>a</sup>, Di Kang<sup>a</sup>, Yiqun Wu<sup>\*ab</sup>, Zhimin Chen<sup>a</sup>, Chunying He<sup>a</sup>, Xin Zhou<sup>\*c</sup>

<sup>a</sup> Key Laboratory of Functional Inorganic Material Chemistry, Ministry of Education, School of Chemistry and Materials Science, Heilongjiang University, Harbin 150080, P. R. China.

<sup>b</sup> Shanghai Institute of Optics and Fine Mechanics, Chinese Academy of Sciences, Shanghai 201800, P. R. China

<sup>c</sup> MIIT Key Laboratory of Critical Materials Technology for New Energy Conversion and Storage, School of Chemistry and Chemical Engineering, Harbin Institute of Technology, Harbin, P. R. China.

Corresponding author E-mail: wangbin@hlju.edu.cn

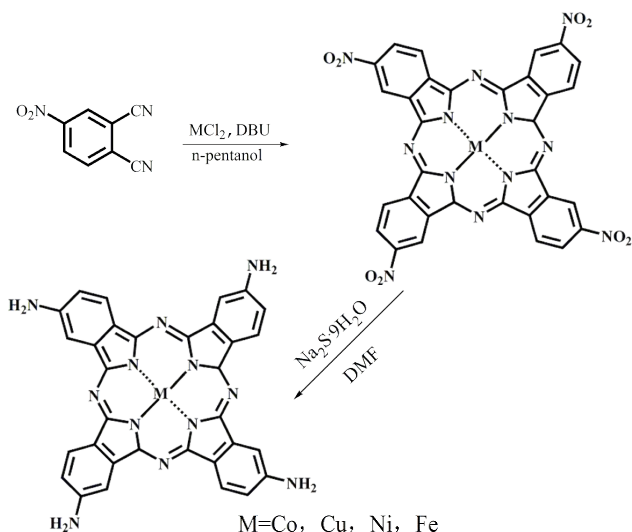
Tel.: +86 451 86609145

Fax: +86 451 86673647

## 1. Experimental detail

### 1.1 Materials

All chemicals were analytical grade and commercially available and used without further purification. 4-nitrophthalonitrile was purchased from Sigma-Aldrich Co . LLC., and was used without further purification. The synthesis scheme of tetra- $\beta$ -aminephthalocyanines metal (II) (aPcMs M= Cu, Ni, Co, Fe) is shown in scheme S1.



Scheme S1. Synthesis scheme of tetra- $\beta$ -aminephthalocyanines metal (aPcMs M= Co, Cu, Ni, Fe).

### 1.2 Characterization

EI and MALDI-TOF mass spectra were performed using an Agilent spectrometer (HP 5973N) and a Bruker microflex LT (Bruker Daltonics, Bremen, Germany) mass spectrometer, respectively. UV/Vis absorption spectra were recorded with a Lambda 35 UV/VIS spectrometer (Perkin-Elmer, USA). FT-IR spectra were recorded on a Nicolet FT-IR NEXUS spectrometer (Thermo Scientific).

### 1.3 Synthesis of tetra- $\beta$ -aminephthalocyanine metal (aPcM)

Tetra- $\beta$ -aminephthalocyanine metal (aPcMs M= Cu(II), Ni(II), Co(II), Fe(II)) were prepared by the same general method: 4-Niyrophthalonitrile (1.0g, 4.7 mmol) was dissolved in 10 ml of anhydrous n-pentanol with anhydrous metal dichloride (1.2 mmol) and 0.4 ml of 1,8-dicyanobicyclo- [5.4.0]-undec-7-ene (DBU). The solution was refluxed for 6h with continuous stirring under a N<sub>2</sub> atmosphere. The reaction mixture was cooled and product was precipitated in methanol solution. The precipitate was suction filtered and washed several times with the dilute hydrochloric acid and sodium hydroxide, and then washed with distilled water until the pH of the

supernatant approached 7. The rough product was washed several times with alcohol and then dried in a vacuum oven at 50 °C to obtained tetra- $\beta$ -nitrophthalocyanine metal. Then, tetra- $\beta$ -nitrophthalocyanine metal was dissolved in DMF with Sodium sulfide. The solution was heated up to 60°C for 2h. The precipitate was washed with ultrapure water until the pH of the supernatant approached 7, and then centrifugal washed with methanol until the centrifugal supernatant is colorless. The product was dried in a vacuum oven at 50 °C to obtained tetra- $\beta$ -aminephthalocyanine metal.

Tetra- $\beta$ -aminephthalocyanine Co (aPcCo): Electronic absorption spectrum (UV-Vis) in DMF: max (nm) = 714, 646. FT-IR spectra (KBr pellets) v: 3338, 3216, 1605, 1494, 1347, 830, 746 cm<sup>-1</sup>. MALDI-TOF-MS (Fig S1A) Calcd (found): m/z = 631.31 (631.51) [M<sup>+</sup>].

Tetra- $\beta$ -aminephthalocyanine Cu (aPcCu): Electronic absorption spectrum (UV-Vis) in DMF: max (nm) = 719, 645. FT-IR spectra (KBr pellets) v: 3319, 3203, 1599, 1496, 1385, 836, 746 cm<sup>-1</sup>. MALDI-TOF-MS (Fig S1A) Calcd (found): m/z = 636.38 (636.13) [M<sup>+</sup>].

Tetra- $\beta$ -aminephthalocyanine Ni (aPcNi): Electronic absorption spectrum (UV-Vis) in DMF: max (nm) = 720, 644. FT-IR spectra (KBr pellets) v: 3322, 3210, 1618, 1488, 1353, 799, 750 cm<sup>-1</sup>. MALDI-TOF-MS (Fig S1C) Calcd (found): m/z = 631.18 (631.27) [M<sup>+</sup>].

Tetra- $\beta$ -aminephthalocyanine Fe (aPcFe): Electronic absorption spectrum (UV-Vis) in DMF: max (nm) = 708, 675. FT-IR spectra (KBr pellets) v: 3359, 3197, 1611, 1462, 1322, 824, 746 cm<sup>-1</sup>. MALDI-TOF-MS (Fig S1A) Calcd (found): m/z = 629.05 (629.13) [M<sup>+</sup>].

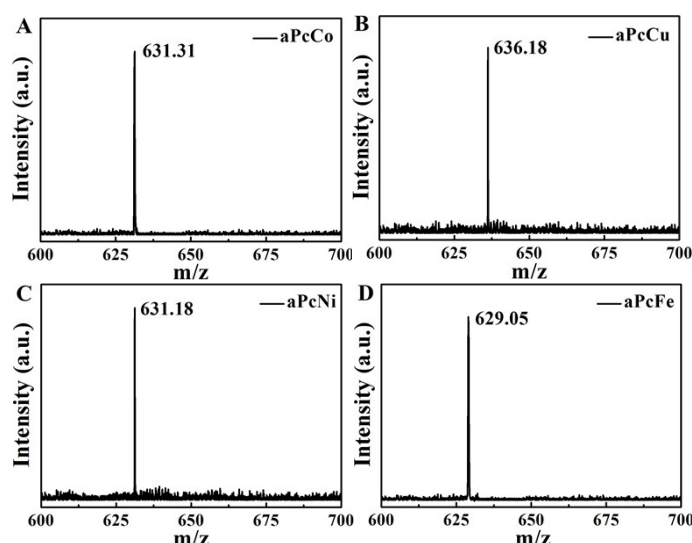


Fig. S1 MALDI-TOF mass spectra of (A) aPcCo-GO, (B) aPcCu-GO, (C) aPcNi-GO, (D) aPcFe-GO.

## Result and discussion

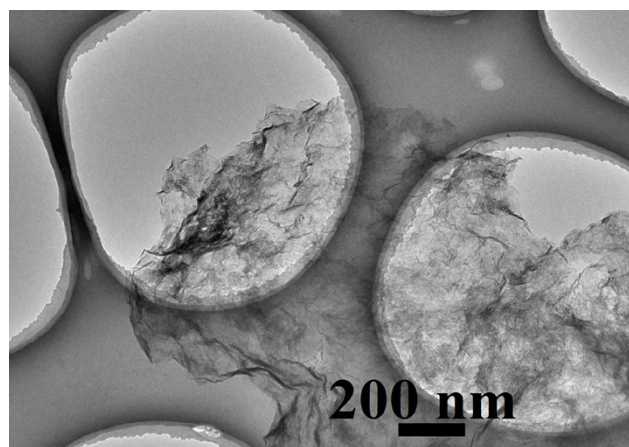


Fig. S2 TEM image of GO

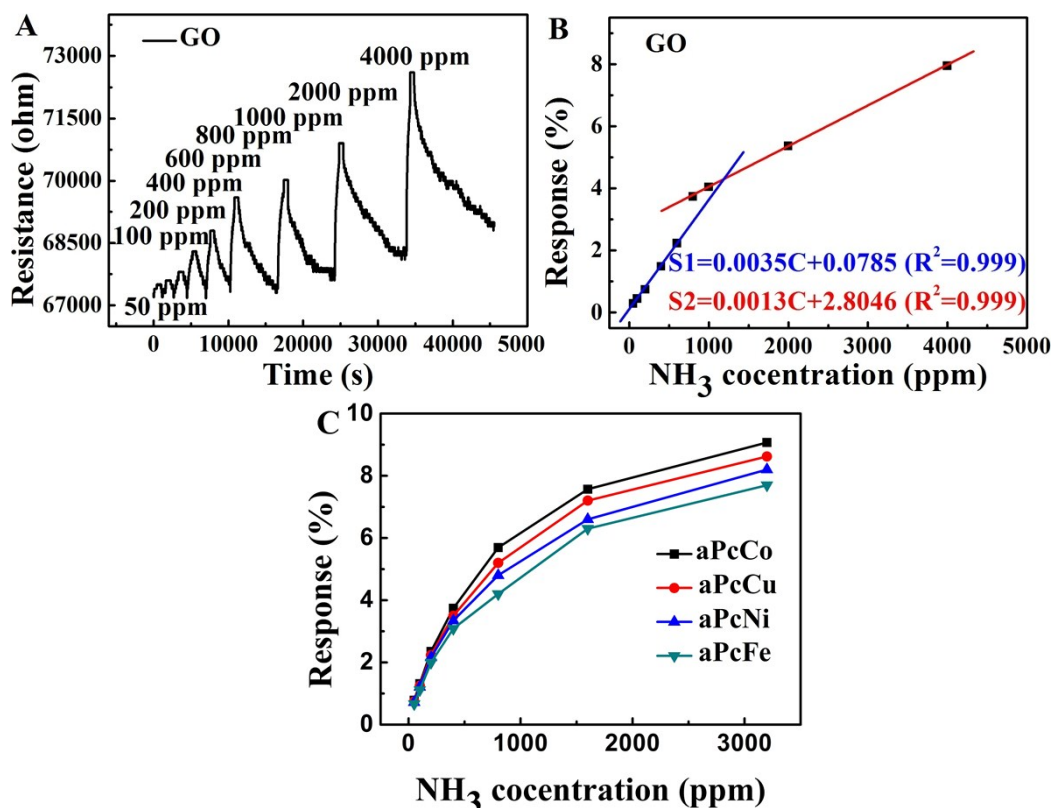


Fig. S3 (A) Resistance of GO sensor upon exposure to varying concentrations of  $\text{NH}_3$ ; relationship of the response of (B) GO and (C) aPcM sensors to the concentration  $\text{NH}_3$ .

Table S1. Comparison of the detection performances of different  $\text{NH}_3$  sensors

| Sensor material                    | Response(%)/Detection conc.<br>(ppm) <sup>[b]</sup> | Detection limit(ppm) <sup>[a]</sup> | Working temperature (°C) <sup>[c]</sup> | Response time(s)/Detection conc.(ppm) <sup>[b]</sup> | Recovery time (s)/Detection conc.(ppm) <sup>[b]</sup> | Detection range (ppm) | Ref. |
|------------------------------------|---|-------------------------------------|---|--|---|-----------------------|------|
| CuO nanowires                      | 3.1/100   | 10                                  | 200                                     | 360/100  | 1800/100  | 10-100                | 1    |
| five-layer MoS <sub>2</sub> sheets | ~20/100   | —                                   | RT                                      | ~300/100   | >600/100 (not fully)                                  | 100-1000              | 2    |

|   |          |      |     |           |                              | recover) |    |
|---|----------|------|-----|-----------|------------------------------|----------|----|
| NiO nanowires   | ~30/100  | —    | 400 | ~36/50    | ~600/50                      | 50-200   | 3  |
| Macroporous WO <sub>3</sub>                                 | —        | 6.2  | 225 | 1200/74   | ~6000/74                     | 6.2-74   | 4  |
| Pt-WO <sub>3</sub>  | 2.7/2.5  | 0.62 | 225 | ~3600/5   | ~3600/5                      | 0.62-5   | 5  |
| Ag-doped - Fe <sub>2</sub> O <sub>3</sub> /SiO <sub>2</sub> | 20/0.1   | 0.1  | RT  | 125/4     | 380/4                        | 0.1-100  | 6  |
| Zn-doped NiO  | 40/50    | 5    | RT  | 5/50      | 30/50                        | 5-150    | 7  |
| CeO <sub>2</sub> @PANI                                      | 6.5/50   | 2    | RT  | 57.6/50   | 300/50                       | 2-400    | 8  |
| PE-co-GMA nanofibers  | 2496/25  | 0.1  | RT  | 75/1      | 600/25                       | 0.1-25   | 9  |
| PANI/Ag nanotubes   | 3/100    | 5    | RT  | ~3000/100 | ~3000/100                    | 5-100    | 10 |
| RGO   | 5.5/200  | 200  | RT  | 900       | >1200/200(not fully recover) | 200-2800 | 11 |
| Graphene  | 100/1000 | 0.5  | RT  | 3600      | 3600                         |          | 12 |
| Phosphorus doped graphene nanosheets                        |          |      |     |           |                              |          | 13 |
| SWCNTs on weighing paper                                    | ~1.5/5   | 0.36 | RT  | 200/5     | >900/5(not fully recover)    | 0.5-80   | 14 |
| CNT-on-paper  | ~2.8/100 | ~5   | RT  | 60/100    | >4/100(not fully recover)    | 10-100   | 15 |
| Au-coated CNT yarn  | ~2.0/50  | 0.5  | RT  | >300/50   | 2700/50                      | 0.5-500  | 16 |
| PANi@CNT  | —        | 50   | RT  | ~1200/50  | —                            | 50-5000  | 17 |

---

|                         | film     |      |    |                     |              |         |      |     |
|-------------------------|----------|------|----|---------------------|--------------|---------|------|-----|
| MWCNTs/SnO <sub>2</sub> | 12/10000 | —    | RT | ~300/10000          | unrecoverabl | e       | —    | 18  |
| /Ag                     | 5/3.0    |      |    |                     |              |         |      |     |
| aPcCo-GO                | 6.5/12.5 | 0.8  | RT | 340/3.0,12.5,<br>50 | <350/50      | 0.8-    |      |     |
|                         | 11.6/50  |      |    |                     |              |         | 3200 |     |
| aPcCu-GO                | 2.6/6.0  |      |    | 540/3.0,12.5,<br>50 | <250/50      | 0.8-    | This |     |
|                         | 3.5/12.5 | 0.8  | RT |                     |              |         | 3200 | wor |
|                         | 8.9/50   |      |    |                     |              |         |      | k   |
| aPcNi-GO                | 3.1/12.5 | 12.5 | RT | 580/12.5,50         | 845/50       | 12.5-   |      |     |
|                         | 6.2/50   |      |    |                     |              |         | 3200 |     |
| aPcFe-GO                | 2.6/200  | 50   | RT | 330/50,200          | 95/400       | 50-3200 |      |     |
|                         | 6.1/800  |      |    |                     |              |         |      |     |

---

[a] If the sensor detection limit was not explicitly provided in the original report, then the lowest tested analyte concentration is listed.

[b] If the response (%), response time (s) or recovery time (s) of the sensor was not explicitly provided in the original report, then the estimate from the curve in that report is listed.

[c] RT, abbreviation for room temperature.

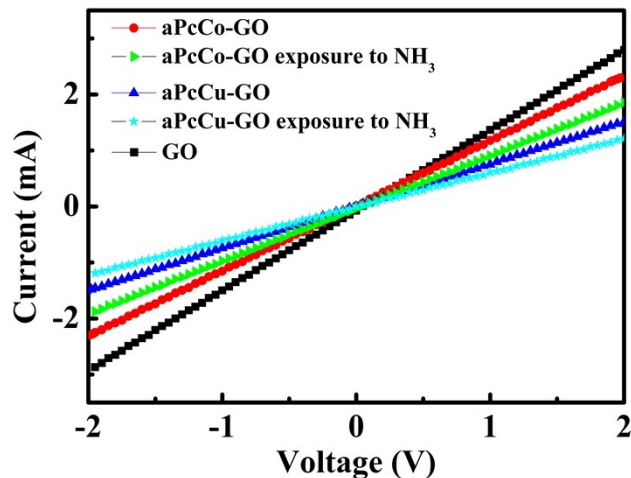


Fig. S4 *I*-*V* curves of the aPcM-GO and aPcM-GO exposure to NH<sub>3</sub>.

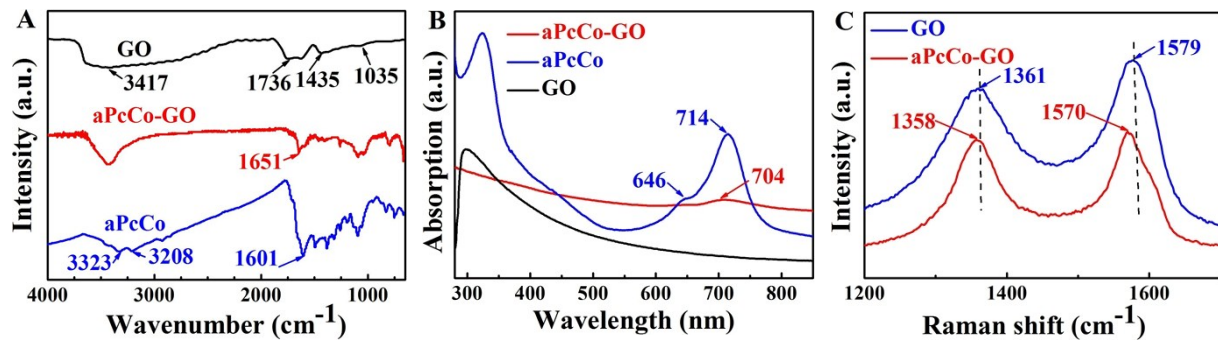


Fig. S5 (A) FT-IR spectra, (B) UV-Vis spectra and (C) Raman spectra of GO and aPcCo-GO hybrid obtained at  $\lambda_{\text{exc}} = 457.9 \text{ nm}$ .

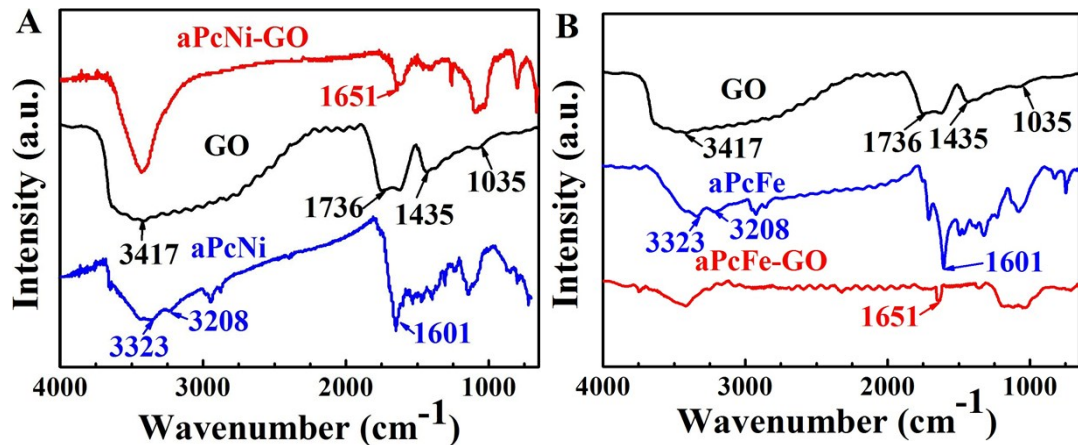


Fig. S6 FT-IR spectra of (A) GO, aPcNi and aPcNi-GO hybrid; (B) GO, aPcFe and aPcFe-GO hybrid.

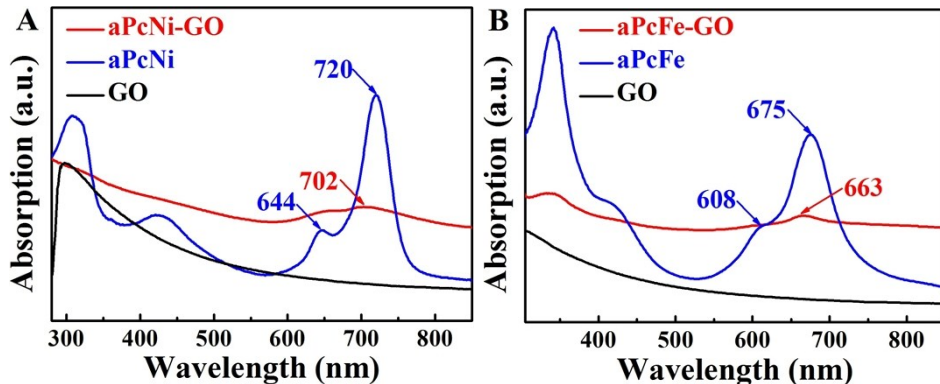


Fig. S7 UV-Vis spectra of (A) GO, aPcNi and aPcNi-GO hybrid; (B) GO, aPcFe and aPcFe-GO hybrid.

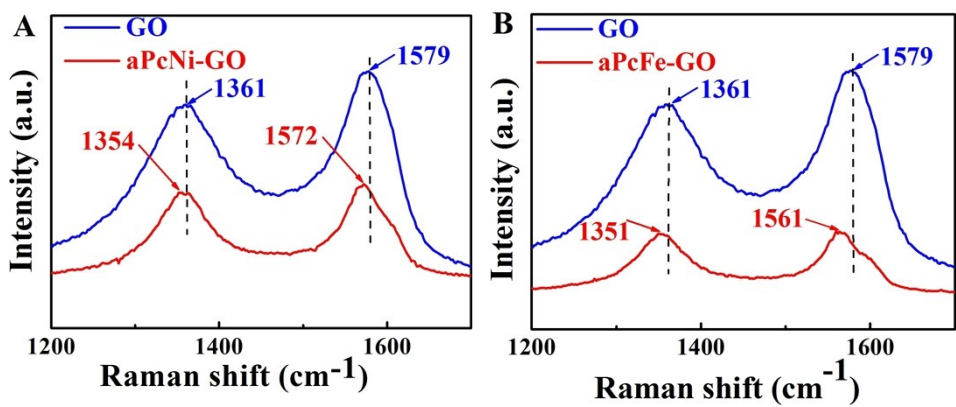


Fig. S8 Raman spectra of (A) GO, aPcNi and aPcNi-GO hybrid; (B) GO, aPcFe and aPcFe-GO hybrid.

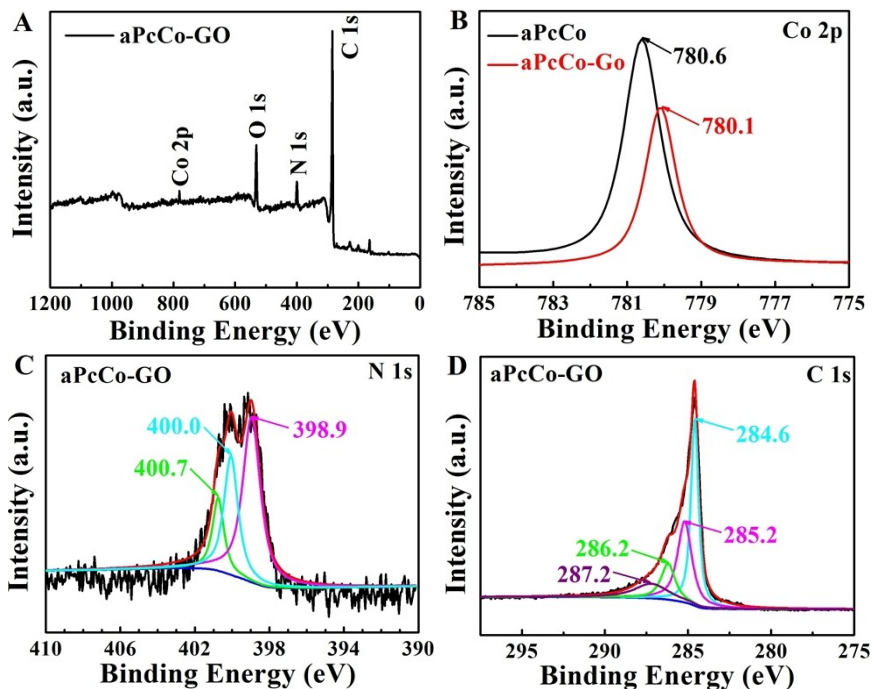


Fig. S9 XPS analysis of aPcCo-GO hybrids: (A) survey spectra; (B) N1s regions; (C) Co 2p region.

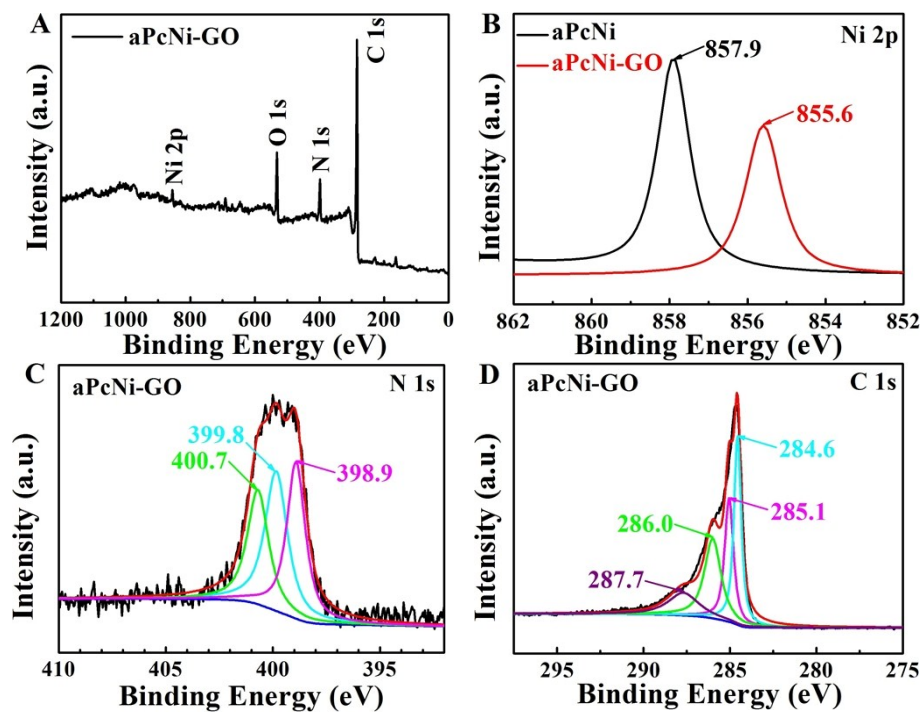


Fig. S10 XPS analysis of aPcNi-GO hybrids: (A) survey spectra; (B) N1s regions; (C) Ni 2p region

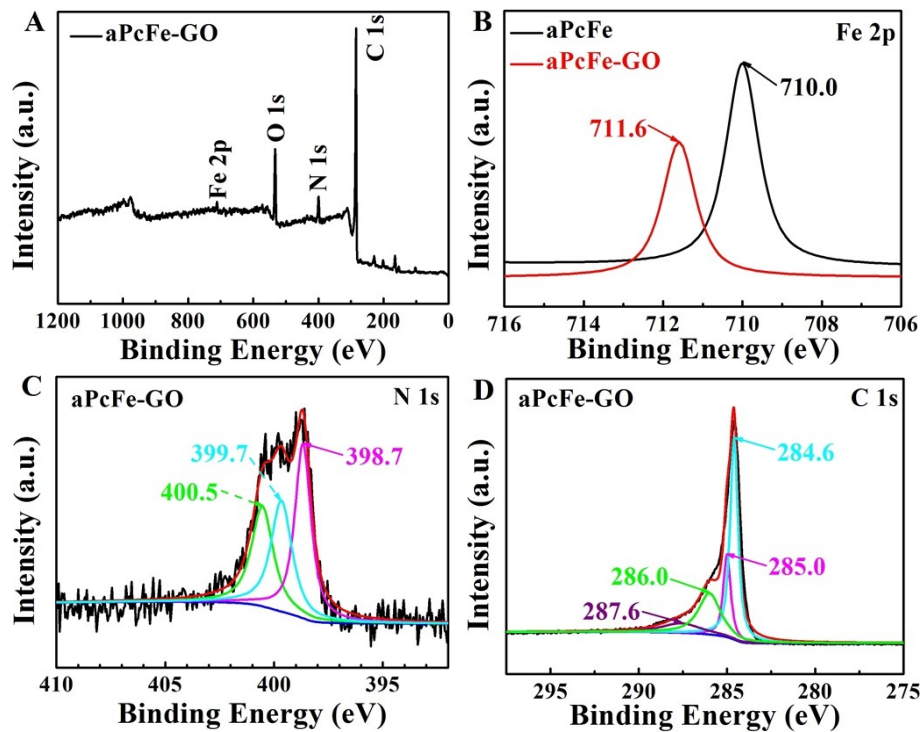


Fig. S11 XPS analysis of aPcFe-GO hybrids: (A) survey spectra; (B) N1s regions; (C) Fe 2p region

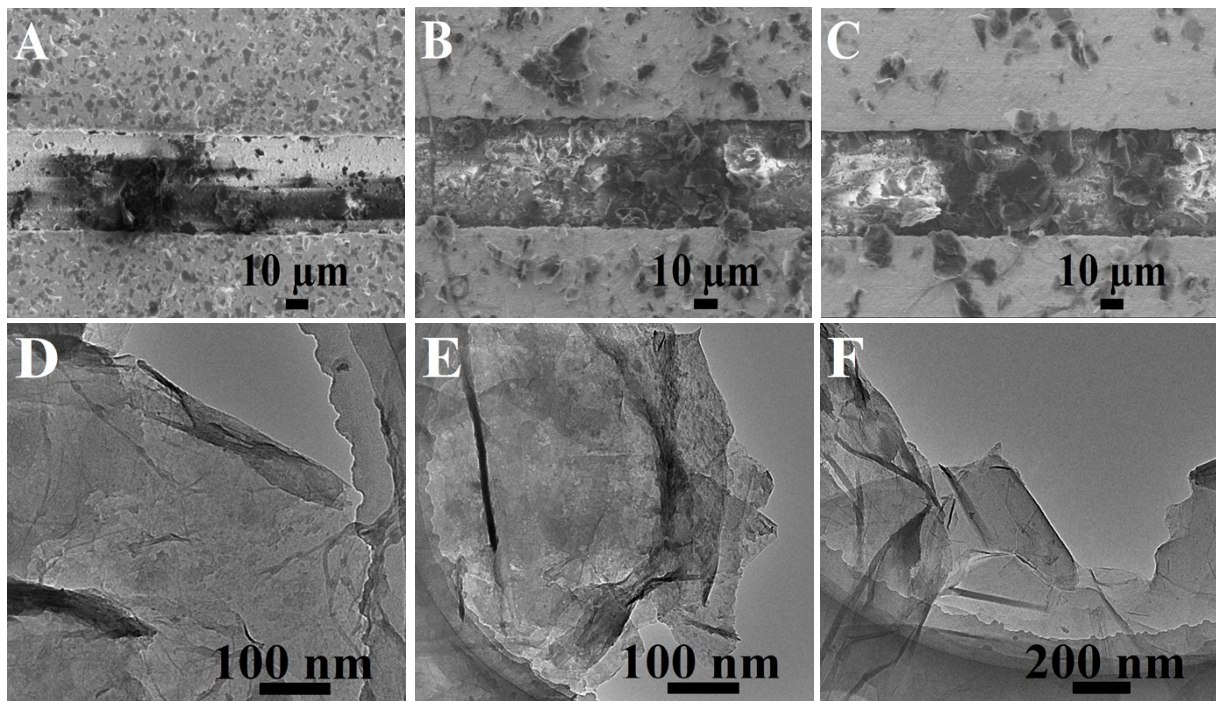


Fig. S12 (A-C) SEM and (D-F) TEM image of (A,D) aPcCo-GO, (B,E) aPcNi-GO and (C,F) aPcFe-GO.

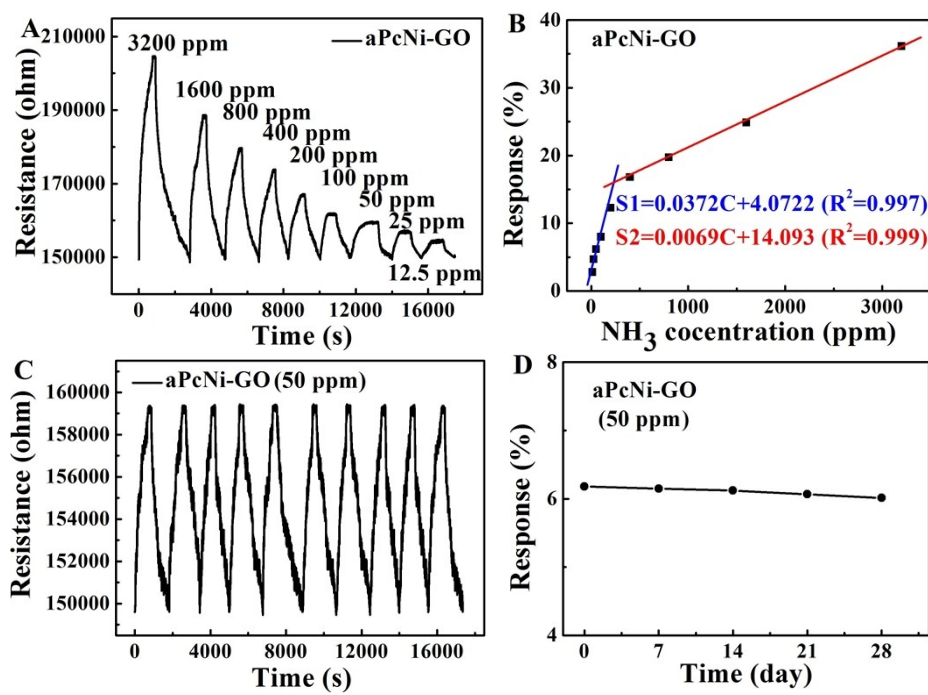


Fig. S13 (a) Response of aPcNi-GO hybrid sensor upon exposure to varying concentrations of NH<sub>3</sub>; (b) relationship of the response of aPcNi-GO sensor to the concentration NH<sub>3</sub>; (c) ten sensing cycles of aPcNi-GO hybrid sensor to 50 ppm NH<sub>3</sub>; (d) response of aPcNi-GO hybrid sensors to 50 ppm NH<sub>3</sub> over long time storage at 28°C.

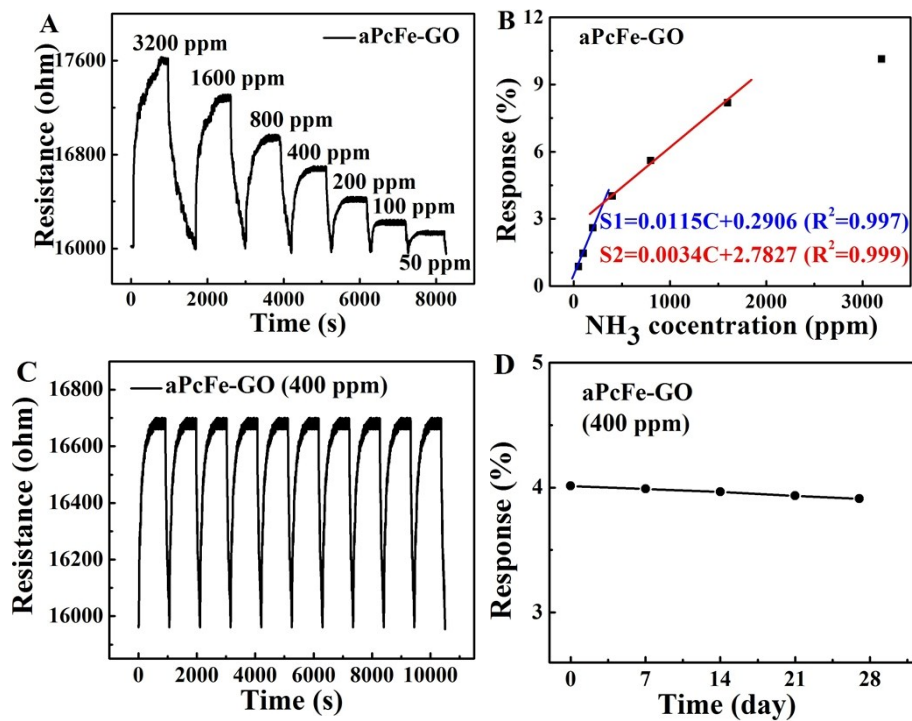


Fig. S14 (a) Response of aPcFe-GO hybrid sensor upon exposure to varying concentrations of NH<sub>3</sub>; (b) relationship of the response of aPcFe-GO sensor to the concentration NH<sub>3</sub>; (c) ten sensing cycles of aPcFe-GO hybrid sensor to 400 ppm NH<sub>3</sub>; (d) response of aPcFe-GO hybrid sensors to 400 ppm NH<sub>3</sub> over long time storage at 28°C.

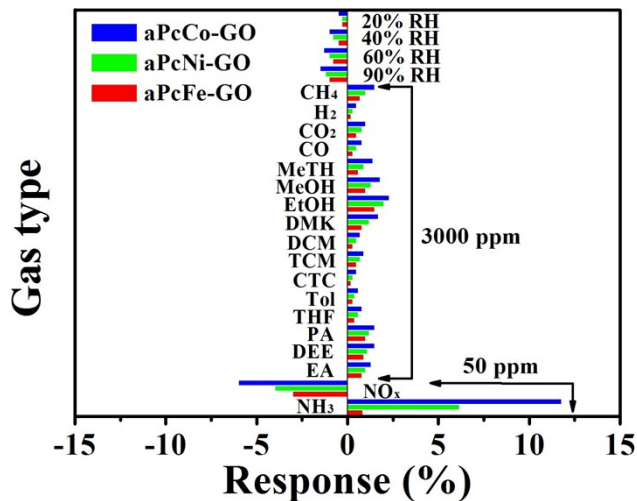


Fig. S15 Cross-sensitivities to various gases for the aPcM-GO sensors at 28°C, MeTH = methanal, MeOH = methanol, EtOH = ethanol, DMK = acetone, DCM = dichloromethane, TCM = trichloromethane, CTC = carbon tetrachloride, Tol = toluene, THF = tetrahydrofuran, PA = propionic acid, DEE = diethyl ether, EA = ethyl acetate.

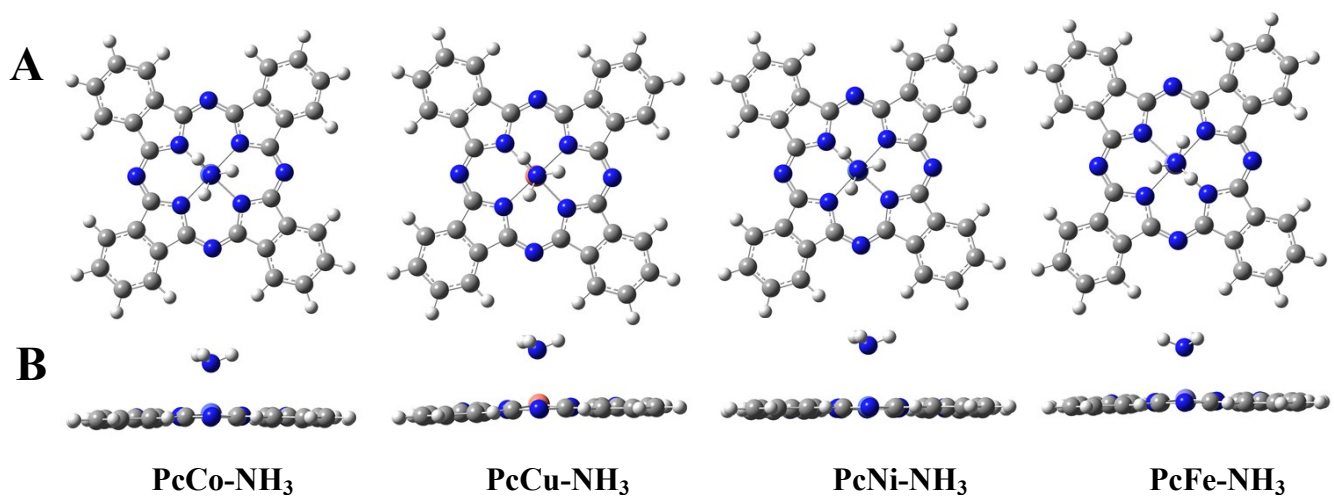


Fig. S16. Optimized structures of NH<sub>3</sub>-aPcMs with (A) top and (B) side views.

## References

1. F. Shao, F. Hernández-Ramírez, J. D. Prades, C. Fàbrega, T. Andreu, J. R. Morante, Copper (II) oxide nanowires for p-type conductometric NH<sub>3</sub>sensing, *Appl. Surf. Sci.*, 311 (2014) 177–181.
2. D. J. Late, Y. Huang, B. Liu, J. Acharya, S. N. Shirodkar, J. J. Luo, A. M. Yan,<sup>†</sup> D. Charles, U. V. Waghmare, V. P. Dravid, C. N. R. Rao, Sensing Behavior of Atomically Thin-Layered MoS<sub>2</sub>, *ACS. Nano.* 7 (2013) 4879–4891.
3. J. Wang, L. M. Wei, L. Y. Zhang, C. H. Jiang, E. S-W. Kong and Y. F. Zhang, Preparation of high aspect ratio nickel oxide nanowires and their gas sensing devices with fast response and high sensitivity, *J. Mater. Chem.* 22 (2012) 8327-8335.
4. M. D'Arienzo, L. Armelao, C. M. Mari, S. Polizzi, R. Ruffo, R. Scotti, F. Morazzoni, Macroporous WO<sub>3</sub> Thin Films Active in NH<sub>3</sub> Sensing: Role of the Hosted Cr Isolated Centers and Pt Nanoclusters, *J. Am. Chem. Soc.* 133 (2011) 5296-5304.
5. C. Zhang, A. Boudiba, M. G. Olivier, R. Snyders, M. Debliquy, Sensing properties of Pt/Pd activated tungsten oxide films grown by simultaneous radio-frequency sputtering to reducing gases, *Sens. Actuators B* 175 (2012) 53-59.
6. Y. L. Tang, Z. J. Li, X. T. Zu, J. Y. Ma, L. Wang, J. Yang, B. Du, Q. K. Yu, Room-temperature NH<sub>3</sub> gas sensors based on Ag-doped -Fe<sub>2</sub>O<sub>3</sub>/SiO<sub>2</sub> composite films with sub-ppm detection ability, *J. Hazard. Mater.* 298 (2015) 154–161.
7. J. Wang, L. M. Wei, L. Y. Zhang, J. Zhang, H. Wei, C. H. Jiang, Y. F. Zhang, Zinc-doped nickel oxide dendritic crystals with fast response and self-recovery for ammonia detection at room temperature, *J. Mater.*

Chem. 22 (2012) 20038.

8. L. L. Wang, H. Huang, S. H. Xiao, D. P. Cai, Y. Liu, B. Liu, D. D. Wang, C. X. Wang, H. Li, Y. R. Wang, Q. H. Li, T. H. Wang, Enhanced Sensitivity and Stability of Room-Temperature NH<sub>3</sub> Sensors Using Core–Shell CeO<sub>2</sub> Nanoparticles@Cross-linked PANI with p–n Heterojunctions, ACS Appl. Mater. Interfaces. 6 (2014) 14131–14140.
9. S. Chen, G. Sun, High Sensitivity Ammonia Sensor Using a Hierarchical Polyaniline/Poly(ethylene-co-glycidyl methacrylate) Nanofibrous Composite Membrane, ACS Appl. Mater. Interfaces. 5 (2013) 6473–6477.
10. X. Li, Y. Gao, J. Gong, L. Zhang, L. Y. Qu, Polyaniline/Ag Composite Nanotubes Prepared through UV Rays Irradiation via Fiber Template Approach and their NH<sub>3</sub> Gas Sensitivity, J. Phys. Chem. C 113 (2009) 69–73.
11. R. Ghosh, A. Midya, S. Santra, S. K. Ray, P. K. Guha, Chemically Reduced graphene Oxide for Ammonia Detection at Room Temperature, ACS. Appl. Mater. Interfaces 5 (2013) 7599–7603.
12. F. Yavari; E. Castillo; H. Gullapalli; P. M. Ajayan; N. Koratkar. High sensitivity detection of NO<sub>2</sub> and NH<sub>3</sub> in air using chemical vapor deposition grown graphene. Appl. Phys. Lett. 100 (2012) 203120-203120-4.
13. F. Niu, L. M. Tao, Y. H. Deng, Q. H. Wang, W. G. Song. Phosphorus doped graphene nanosheets for room temperature NH<sub>3</sub> sensing. New J Chem. 38 (2014) 2269–2272.
14. K. A. Mirica, J. G. Weis, J. M. Schnorr, B. Esser and T. M. Swager, Mechanical Drawing of Gas Sensors on Paper, Angew. Chem. Int. Ed. 51 (2012) 10740-10745.
15. J. W. Han, B. Kim, J. Li, M. Meyyappan, A carbon nanotube based ammonia sensor on cellulose paper, RSC Adv. 4 (2014) 549-553.
16. Lakshman K. Randeniya, Philip J. Martin, Avi Bendavid, Jill McDonnell, Ammonia sensing characteristics of carbon-nanotube yarns decorated with nanocrystalline gold, Carbon 49 (2011) 5265-5270.
17. Z. P. Liu, G. M. Liao, S. Y. Li, Y. Y. Pan, X. Y. Wang, Y. Y. Weng, X. H. Zhang and Z. H. Yang, Efficient encapsulation of conducting polyaniline chains inside carbon nanotubes: a new strategy to prepare endohedral CNT materials, J. Mater. Chem. A 1(2013) 13321-13327.
18. S. M. Cui, H. H. Pu, E. C. Mattson, G. H. Lu, S. Mao, M. Weinert, C. J. Hirschmugl, M. Gajardziska-Josifovska and J. H. Chen, Ag nanocrystal as a promoter for carbon nanotube-based room-temperature gas sensors, Nanoscale 4 (2012) 5887-5894.